SANS Study on Pressure-Induced Phase Separation of Poly(*N*-isopropylacrylamide) Aqueous Solutions and Gels

Mitsuhiro Shibayama,* Kohji Isono, Satoshi Okabe, Takeshi Karino, and Michihiro Nagao

Neutron Science Laboratory, Institute for Solid State Physics, The University of Tokyo, 106-1 Shirakata, Tokai, Ibaraki 319-1106, Japan

Received December 21, 2003; Revised Manuscript Received February 14, 2004

ABSTRACT: Pressure-induced phase separation of poly(*N*-isopropylacrylamide) (PNIPA) aqueous solutions and gels were investigated by small-angle neutron scattering (SANS). The cloud point curves were constructed on the pressure−temperature ($P-T$) plane by visual observation for both the solutions and gels. As observed in the phase diagram of aqueous solutions of proteins, the cloud point temperatures (T_{cloud}) were a function of the pressure, P, and had maxima at $P_0 = 51.7$ MPa and $P_0 = 93.2$ MPa respectively for the solution and gel in H_2O. The difference in T_{cloud} indicates that the effect of cross-linking is significant, and it leads to an increase of the miscible region. The SANS intensity function for the solution was well represented by a Lorentz function, i.e., an Ornstein−Zernike (OZ) function, from which the correlation length, ξ, and the susceptibility, $I(0)$, were evaluated as a function of pressure. The critical exponents were obtained to be $1.1 \leq \gamma_p \leq 1.23$ and $0.5 \leq \nu_p \leq 0.6$, for the solution, similar to the case of the temperature dependence of ξ and $I(0)$. The spinodal temperature, T_{sp}, seems to merge with the binodal curve (T_{clould}) at P_0 for the PNIPA solution. $I(q)$'s for the gels, on the other hand, deviated significantly from an OZ form by approaching the spinodal and were well fitted with a sum of squared-Lorentz and Lorentz functions. This squared-Lorentz function accounts for the emergence of cross-link inhomogeneities, which become dominant near the spinodal. These structure changes by pressure will be discussed in conjunction with cold denaturation of proteins.

Introduction

Poly(*N*-isopropylacrylamide) (PNIPA) gels are known to be environment-sensitive gels.[1,2] Upon a slight change of an environmental variable, such as temperature,[3,4] solvent composition,[5,6] or hydrostatic pressure,[7−9] PNIPA gels undergo either a swelling or a shrinking transition. The environment sensitivity is mainly ascribed to the strong hydrophobicity of the *N*-isopropyl groups located on the side chain. At lower temperatures (e.g., less than 32 °C), water molecules around the *N*-isopropyl groups are ordered and form an iceberg structure[10] in order to minimize the number of contact with the hydrophobic groups.

In contrast to the temperature dependence, the pressure dependence is more sophisticated as discussed by Otake et al.[11] for PNIPA solutions and by Kato and coworkers[12] and Nakamoto et al.[9] for PNIPA gels. According to Kato, the Flory interaction parameter, χ, is a quadratic function of pressure, P, which results in a reentrant swelling−shrinking transition as P is increased. Rebelo et al. discussed double critical phenomena of PNIPA aqueous solutions and PNIPA-*co*-poly(1-deoxy-1-methacrylamide-D-glucitol).[13] They demonstrated that the phase behavior of PNIPA aqueous solutions has a saddlelike landscape in the $P-T-\phi$ phase diagram, where ϕ is the volume fraction of the polymer. Kunugi reported an elliptic-shape phase diagram in the $P-T$ plane for PNIPA aqueous solutions and discussed the behavior as an analogy of cold denaturation of proteins at high pressure.[14,15]

An introduction of cross-links leads to an increase of inhomogeneities, topological memory effects, reduction of chain mobility, etc.[16] The inhomogeneities themselves can be classified into various categories, such as spatial inhomogeneities, topological inhomogeneities, and connectivity inhomogeneities. In this study, we discuss (1) the effects of pressure on the phase separation thermodynamics of PNIPA solutions and gels, (2) the role of cross-links in the structure factor of polymer gels, and (3) critical phenomena of polymer solutions and gels in the $P-T$ plane. The goal of this study is to elucidate the pressure and temperature dependence of hydrophobic interactions in aqueous solutions of water-soluble polymers, including proteins. The dynamics near the spinodal will be reported in a separate paper.

Theoretical Background

Scattering Intensity for Polymer Solutions. The scattering intensity for polymer solutions in the semidilute regime is given by a Lorentzian (or Ornstein−Zernike) function, i.e.

$$I(q) = \frac{K_{NS}}{v_1}\frac{\phi^2 k_B T N_A}{K_{os}}\frac{1}{1+\xi^2 q^2} \tag{1}$$

where k_B is the Boltzmann constant, T the absolute temperature, N_A the Avogadro number, ξ the correlation length, K_{os} the osmotic modulus, and q the momentum transfer (i.e., the magnitude of scattering vector). K_{NS} is the scattering contrast defined by

$$K_{NS} = N_A v_1\left[\left(\frac{b_2}{v_2}\right) - \left(\frac{b_1}{v_1}\right)\right]^2 \tag{2}$$

where v_i and b_i are the molar volume and the scattering length of the solvent molecule ($i = 1$) and the solute ($i = 2$), respectively. Here, K_{NS} has the unit of cm^{-1},

* To whom correspondence should be addressed: e-mail sibayama@issp.u-tokyo.ac.jp.

10.1021/ma0359685 CCC: $27.50
Published on Web 03/23/2004

equivalent to that of the absolute intensity. In the case of a D_2O solution of PNIPA, the contrast factor is estimated to be $K_{NS} = 9.21 \times 10^{-2}$ cm^{-1}. The correlation length is related to

$$\xi^2 = \frac{k_B T \phi^2}{K_{os}} \frac{1}{12\phi(1-\phi)\zeta} = \frac{k_B T \phi}{K_{os}} \frac{1}{12(1-\phi)\zeta} \quad (3)$$

where ζ is the segment length. The osmotic modulus is given by

$$K_{os} = \frac{k_B T N_A \phi^2}{v_2}\left[\frac{1}{N\phi} + \frac{1}{1-\phi} - 2\chi\right] \quad (4)$$

Here, χ is the interaction parameter, we take the reference volume to be that of the solute since the degree of polymerization, N, is defined with respect to the solute volume and not to the solvent volume.

Scattering Intensity for Polymer Gels. If a polymer solution is cross-linked without perturbing the polymer chain conformation, the osmotic modulus is modified by taking account of the shear modulus. The scattering intensity, $I(q)$, is then given by

$$I(q) = \frac{K_{NS}}{v_1} \frac{k_B T \phi^2 N_A}{M_{os}} \frac{1}{1+\xi^2 q^2} \quad (5)$$

where M_{os} is the longitudinal osmotic modulus of the gel and is given by

$$M_{os} \equiv K_{os} + \frac{4\mu}{3} \quad (6)$$

where μ is the shear modulus. If this is the case, $I(q)$ for a gel is weaker than the corresponding polymer solution since μ is positive. However, in reality, $I(q)$ for a gel is stronger due to emergence of cross-linking inhomogeneities.

When cross-links are introduced to a polymer solution in semidilute regime, $I(q)$ is perturbed. According to Panyukov and Rabin,[17] the structure factor, $S(q)$, and $I(q)$ are given by

$$S(q) \equiv \overline{\langle \rho_{\mathbf{q}} \rho_{-\mathbf{q}} \rangle} = G(q) + C(q) = \frac{g_{\mathbf{q}}}{1 + w g_{\mathbf{q}}} + \frac{v_{\mathbf{q}}}{(1 + w g_{\mathbf{q}})^2} \quad (7)$$

and

$$I(q) = K_{NS} \phi N_X S(q) \quad (8)$$

where N_X is the average number of monomers between cross-links. Hence, $S(q)$ consists of the thermal correlator $G(q)$ and the square of $G(q)$.

$g(q)$ is given by

$$g(q) = \frac{1}{Q^2/2 + (4Q^2)^{-1} + 1} + \frac{2}{(1+Q^2)^2 (\phi_0/\phi)^{2/3}} \quad (9)$$

Q is the reduced scattering vector normalized by the monomer fluctuating radius, i.e., $Q \equiv (a N_X^{1/2}/\sqrt{6})q$ and ϕ_0 is the volume fraction of the gel at sample preparation. The term $(4Q^2)^{-1}$ in the denominator of the first term of the right-hand side of eq 9 is due to the cross-linking as first introduced by de Gennes for heteropolymer networks.[18] On the other hand, the static correlator, which corresponds to the contribution from the frozen structure of gels, is given by

$$C(q) = \frac{\phi N_X}{[1 + w g(q)]^2 (1+Q^2)^2}\left[6 + \frac{9}{w_0 - 1 + (1/2)Q^2\left(\frac{\phi_0}{\phi}\right)^{2/3}}\right] \quad (10)$$

where w_0 and w are the excluded-volume parameters at sample preparation and at observation, respectively

$$w_0 = (1 - 2\chi_0 + \phi_0)\phi_0 N_X \quad (11)$$

$$w = (1 - 2\chi + \phi)\phi N_X \quad (12)$$

In the case of polymer solutions, $C(q)$ is absent. In addition, the second term of eq 9 and the cross-linking term are not necessary. In this case, eq 8 is reduced to eq 1, and one obtains

$$\xi = \sqrt{\frac{a^2}{12(1 - 2\chi + \phi)\phi N_X}} \quad (13)$$

For as-prepared gels away from its critical saturation threshold, the following relation can be obtained by substituting $\phi = \phi_0$ and $w_0 \gg 1$.

$$S_{\mathbf{q}} \cong \frac{S_L(0)}{1+\xi^2 q^2} + \frac{S_{SL}(0)}{(1+\xi^2 q^2)^2} \quad (14)$$

The derivation is given in the Appendix. Therefore, the scattering function for as-prepared polymer gels is given by a sum of Lorentz and squared-Lorentz functions.

Onuki also derived a structure factor for isotropically swollen gels[19,20]

$$I(q) \cong \frac{K_{NS}}{v_1} \frac{k_B T N_A \phi^2}{M_{os}} \times \left[\frac{1}{1+\xi^2 q^2} + p(q)\left(\frac{\phi_0}{\phi}\right)^{2/3} \frac{\mu}{K_{os} + 4\mu/3} \frac{1}{(1+\xi^2 q^2)^2}\right] \quad (15)$$

where $p(q)$ is the Fourier transform of the autocorrelation of the cross-link density deviation.[20] In the case that the cross-link is randomly distributed in the space obeying a Poisson distribution, $p(q)$ can be set as a constant, i.e., $p(q) = p_{int}$. Hence, eq 15 can be approximated to be a linear combination of Lorentz (L) and squared-Lorentz (SL) functions, i.e.

$$I(q) = \frac{I_L(0)}{1+\xi^2 q^2} + \frac{I_{SL}(0)}{(1+\xi^2 q^2)^2} \quad (16)$$

where $I_L(0)$ and $I_{SL}(0)$ are the zero-q intensities corresponding to the dynamic and static contributions to $I(q)$. Note that there is only one characteristic length, i.e., ξ, in eq 16. A similar functional form was also introduced by Geissler and co-workers, which is a linear combination of the SL and L terms, but they introduced two independent correlation lengths corresponding to the SL and L terms, e.g., Ξ and ξ.[21] Such an approach may be valid if the gel consists of a mixture of two different gels or a gel and a solution. On the other hand, the

Panyukov−Rabin theory and Onuki theory describe the structure factor of polymer gels with only one length parameter, ξ. In this paper, we use eq 16 for the analysis of the temperature and pressure dependence of the structure factors of gels although the Onuki theory cannot be applied near the instability point because the theory is based on a perturbation theory.[20]

Critical Exponents. As is the case of magnetic matter and binary fluids,[22] polymer gels also exhibit critical phenomena. Li and Tanaka reported that a polymer gel is classified to be a three-dimensional Ising model.[23] Shibayama et al. reported the applicability of the following relation to the critical phenomena of polymer solutions and gels[24]

$$\xi = \xi_0 \left| \frac{T - T_{sp}}{T_{sp}} \right|^{-\nu} \tag{17}$$

$$I(0) = I_0(0) \left| \frac{T - T_{sp}}{T_{sp}} \right|^{-\gamma} \tag{18}$$

where T_{sp} is the spinodal temperature and ξ_0 and $I_0(0)$ are constants. It is well-known that the critical exponents are $\nu = 0.5$ and $\gamma = 1.0$ for the mean field and $\nu = 0.63$ and $\gamma = 1.23$ for the Ising model.[22] We assume here that a similar relationship is obtained regarding the pressure dependence

$$\xi = \xi_0 \left| \frac{P - P_{sp}}{P_{sp}} \right|^{-\nu_P} \tag{19}$$

$$I(0) = I_0(0) \left| \frac{P - P_{sp}}{P_{sp}} \right|^{-\gamma_P} \tag{20}$$

where ν_P and γ_P are the critical exponents for the pressure dependence of ξ and $I(0)$, respectively, and P_{sp} is the spinodal pressure.

Experimental Section

Poly(*N*-isopropylacrylamide) (PNIPA) gels were prepared with 690 mM recrystallized *N*-isopropylacrylamide monomer, 8.62 mM bis(acrylamide), 1.75 mM ammonium persulfate, and 8.0 mM *N*,*N*,*N*′,*N*′-tetramethylethylenediamine. A pregel solution of either H_2O or D_2O was degassed and then polymerized in a pressure cell at 20 °C and atomospheric pressure. PNIPA aqueous solutions were also made with the same recipe but without adding bis(acrylamide). Cloud point measurements for PNIPA solution and gel were carried out by visual observation at the scattering angle of 90° for the samples installed in a pressure cell (PCI-400-4W, Telamex, Co., Ltd., Kyoto) equipped to a static/dynamic light scattering apparatus, ALV-5000 (Langen, Germany). The temperature of the sample was regulated by circulating water from a NESLAB RTE-111 thermocontroller with the precision of ±0.1 °C.

Pressure-dependent SANS experiments were carried out at the SANS-U, owned by the University of Tokyo, placed at the JRR-3M reactor guide hall, Japan Atomic Energy Research Institute. The wavelength of the neutron was monochromatized to be 7.0 Å with a velocity selector with the wavelength distribution of 13%.[25] The sample-to-detector distance was 4.00 m, which allowed the experimental q range to be 0.01−0.08 Å^{-1}. Pressure-dependent SANS experiments were conducted with a high-pressure cell, PCI-400-SANS (Teramex, Co. Ltd., Kyoto, Japan). The PCI-400-SANS is an inner cell-type pressure cell, which was designed to isolate the sample from the pressurizing medium.[26] The basic concept of the pressure cell is described elsewhere.[27] The inner cells have quartz windows 2 mm thick. The applied pressure is transmitted via a rubber diaphragm connected to the inner cell. The outer chamber was filled with D_2O, and the pressure was controlled by pressurizing D_2O by a double-cylinder hand pump. The same temperature controller was used to regulate the temperature of the SANS. The scattered intensity was counted with a two-dimensional position-sensitive detector and circularly averaged, followed by several corrections, such as air, cell, and solvent scatterings, and transmission, before normalizing to the absolute intensity with an intensity calibration standard sample. For the calibration, a secondary standard sample, i.e., a polyethylene slab (Lupolen), was used, which was calibrated with the incoherent scatering of vanadium (the primary standard).[28]

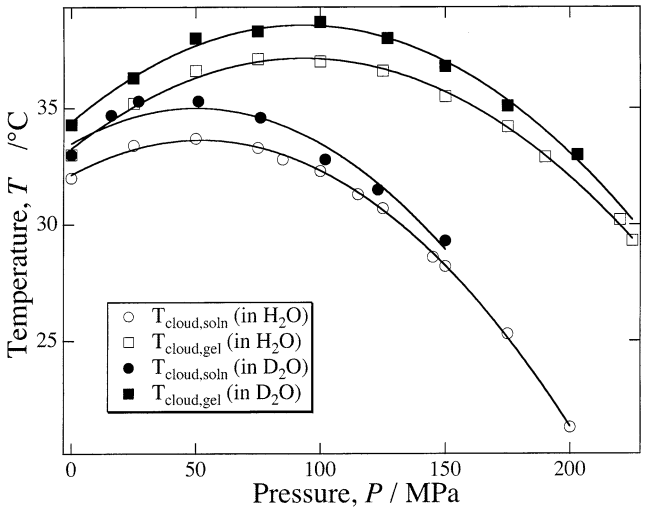

Figure 1. Phase diagram of 690 mM PNIPA solution and gel. The cross-linker concentration was 8.62 mM. The solid lines are drawn by the curve-fitting with a parabolic function.

Results and Discussion

Phase Diagram. Figure 1 shows the cloud point curves for PNIPA solution (filled and open circles) and gel (filled and open squares) in H_2O (open symbols) and in D_2O (filled symbols). The polymer concentration was 7.8 wt %. The cloud point pressure was determined by visual observation of the scattered light at 90° and was also confirmed by photon detection. The cloud point was very reproducible and reversible with respect to both temperature and pressure. The phase diagrams can be fitted with a quadratic function given by

$$T_{cloud,soln} = -5.59 \times 10^{-4} \times (P - 51.7\ [\mathrm{MPa}])^2 + 33.6\ [^\circ\mathrm{C}]\ (H_2O)$$

$$T_{cloud,gel} = -4.46 \times 10^{-4} \times (P - 93.2\ [\mathrm{MPa}])^2 + 37.1\ [^\circ\mathrm{C}]\ (H_2O)$$

$$T_{cloud,soln} = -5.99 \times 10^{-4} \times (P - 48.2\ [\mathrm{MPa}])^2 + 35.3\ [^\circ\mathrm{C}]\ (D_2O)$$

$$T_{cloud,gel} = -4.80 \times 10^{-4} \times (P - 93.0\ [\mathrm{MPa}])^2 + 38.6\ [^\circ\mathrm{C}]\ (D_2O)$$

where the critical pressures, P_c, and temperatures, T_c, were evaluated to be (P_c, T_c) = (51.7 MPa, 33.6 °C) and (93.2 MPa, 37.1 °C) respectively for the solution and the gel in H_2O. It should be noted the following. This type of phase diagram was also reported by Kunugi for

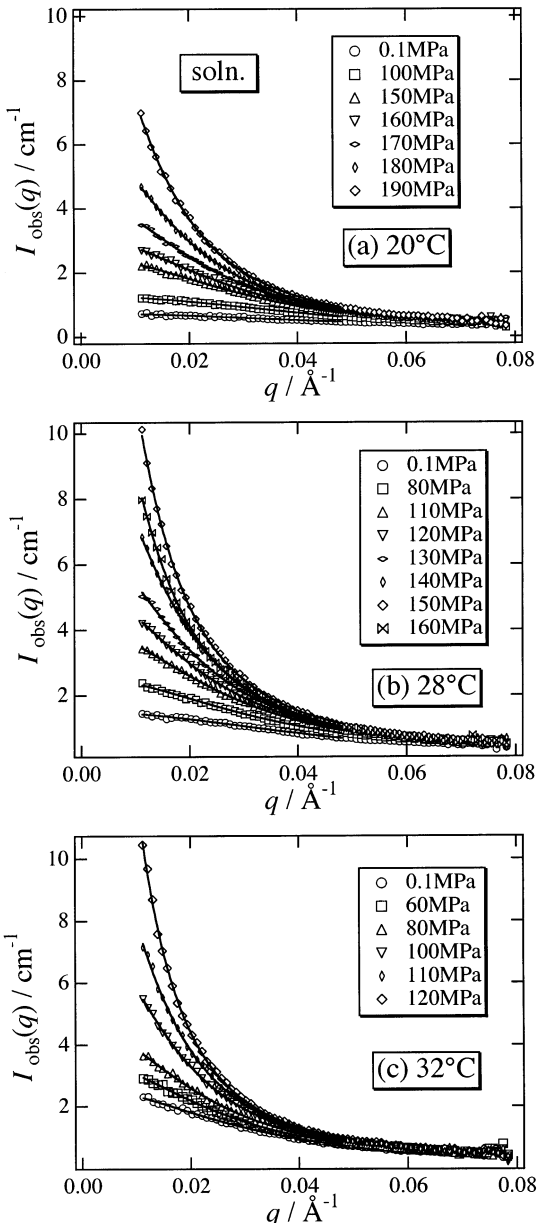

Figure 2. SANS intensity, $I(q)$, for PNIPA solution in D_2O obtained at various pressures at (a) 20, (b) 28, and (c) 32 °C. The solid lines are fits with a Lorentz function (eq 1 in the text).

PNIPA solutions. The reason for the convexity is originated from the negative volume change of mixing at low pressures, and it changes to positive at elevated pressures as recently reported by Kato.[29] In the cases of the solution and the gel in D_2O, the cloud point curves shift upward by about 1.5 deg. This is one of the isotope effects as observed not only in PNIPA−water phase behavior[24,30] but also in phase separation of polymer blends,[31] polymer crystallization, and others. This effect is mainly due to the molar volume isotope effect as studied by Buckingham and Hentschel.[32] In this study, we focus on the phase diagrams for the D_2O systems since SANS data are mostly investigated.

Pressure and Temperature Dependence of the Structure Factor for PNIPA Solutions. Figure 2 shows $I(q)$'s for 690 mM PNIPA solutions (= 7.8 wt %) in D_2O at (a) 20, (b) 28, and (c) 32 °C. $I(q)$ is a monotonically decreasing function of q, but it increases by increasing pressure, P. The solid line is the fit with

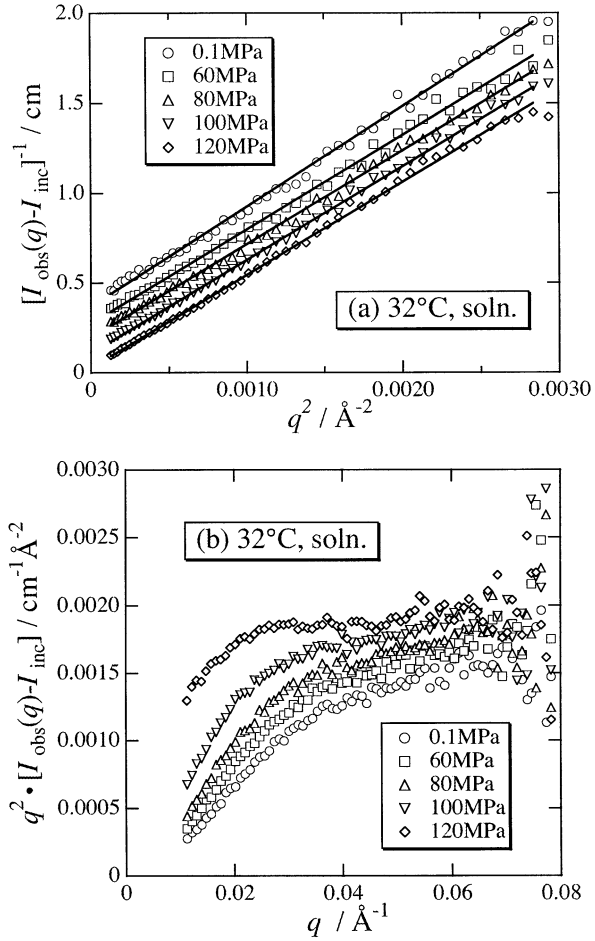

Figure 3. (a) Ornstein−Zernike, $1/[I(q) - I_{inc}]$ vs q^2, and (b) Kratky, $q^2[I(q) - I_{inc}]$, plots for PNIPA solutions at various pressures. The temperature of observation was 32 °C.

eq 1, i.e., a Lorentz function. Note that the scattering intensity was corrected by subtracting incoherent scattering, $I_{inc} = 0.13$ cm^{-1}. This value was obtained by SANS measurement of a 690 mM *N*-isopropylacrylamide monomer solution in D_2O. The fitting is quite successful. This means that the PNIPA solutions can be nicely described as semidilute polymer solutions. The temperature and pressure dependence of the evaluated values for ξ will be discussed later.

Figure 3 shows (a) an Ornstein−Zernike (OZ) plot, i.e., $1/[I(q) - I_{inc}]$ vs q^2, and (b) a Kratky plot for the PNIPA solution at 32 °C. The solid lines indicate the fits with eq 1. The fitting was satisfactory for the PNIPA solution. Susceptibility, $I(0)$, and ξ were obtained from the OZ plots. Note that the Kratky plot shows a leveling off at the high-q region as is commonly observed for polymer solutions in the semidilute regime.

Figure 4 shows the variation of (a) ξ and (b) $I(0)$ for the 690 mM PNIPA solution as functions of P. Both ξ and $I(0)$ increase with increasing P. Interestingly, however, each of the ξ curves shows a cusp at high pressures, e.g., at 150 MPa for 28 °C. This cusp indicates the pressure at which a phase separation takes place before divergence of ξ at the spinodal. In other words, this indicates a binodal. A similar behavior was also observed in the variations of $I(0)$ as a function of P. One of the thermodynamic quantities, i.e., the bulk modulus, K_{os}, is also plotted in Figure 4b, which is on the order of MPa and decreases with increasing P.

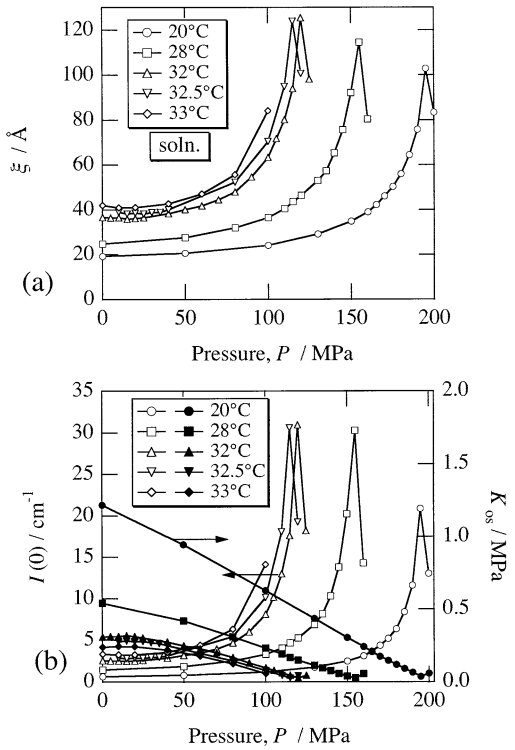

Figure 4. Pressure dependence of (a) the correlation length, ξ, and (b) the susceptibility, $I(q = 0)$, for PNIPA solution. It should be noted that the data show a cusp at an elevated pressure for each temperature, indicating the bimodal point. The osmotic modulus, K_{os}, evaluated with eq 1 is also plotted with the right axis.

It is of interest to evaluate the critical exponents, ν_P and γ_P, for this system. Figure 5 shows the result of fitting with eqs 19 and 20 respectively for ξ and $I(0)$. Here, a three-parameter fitting was carried out by floating (ξ_0, P_{sp}, ν_P) and ($I_0(0)$, P_{sp}, γ_P) respectively for ξ and $I(0)$. As shown in the figure, the fittings were quite successful. The temperature dependence of the obtained critical exponents is shown in Figure 6. Though the data points are somewhat scattered due to the lack of the statistics in the SANS measurements as well as the lack of the sampling points, the observed critical exponents suggest this system being classified to the three-dimensional Ising model as the same as their temperature dependence.[23,24]

Figure 7 shows the $P-T$ phase diagram for PNIPA solution in D_2O obtained by SANS as well as light scattering (LS). The cloud point curve, T_{cloud}, was obtained by LS at a scattering angle of 90°. The binodal temperature, T_b, was determined from the cusp in the $\xi-P$ plot in Figure 4. The spinodal temperature, T_{sp}, was evaluated at which ξ and $I(0)$ diverge, i.e., the temperature at the spinodal pressure, P_{sp}. It is noteworthy that the T_{cloud} curve for PNIPA in D_2O obtained by LS is nicely superimposed to the T_b curve obtained by SANS. In addition, the T_{sp} curve seems to merge the T_b curve at the critical point (P_c, T_c).

Pressure and Temperature Dependence of $I(q)$ for PNIPA Gels. Figure 8 shows (a) the OZ and (b) Kratky plots for $I(q)$'s for the gel, where I_{inc} was corrected. As shown in Figure 8a, the OZ plots have a nonlinear component at low q's, and the curves at high pressures have negative intercepts. Such non-Lorentzian behavior is more clearly observed in the Kratky plot

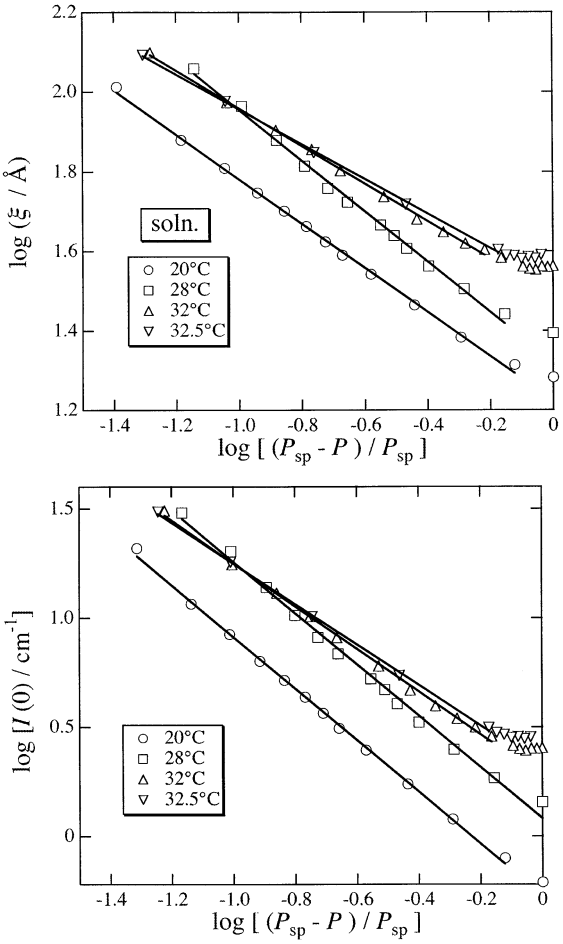

Figure 5. Plots of $\log[\xi/Å]$ vs $\log[P_{sp} - P]/P_{sp}$ and $\log[I(0)/cm^{-1}]$ vs $\log[P_{sp} - P]/P_{sp}$ for PNIPA solution at 20, 28, 32, and 32.5 °C.

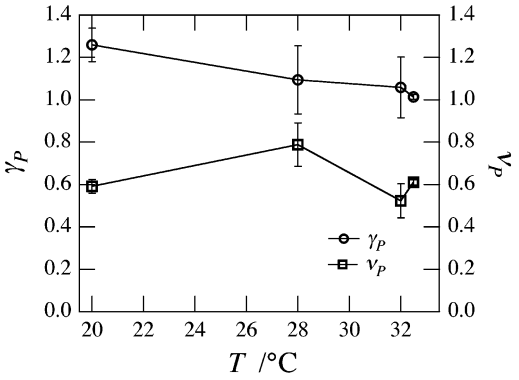

Figure 6. Temperature dependence of the critical exponents, γ_P and ν_P, for PNIPA solution.

(Figure 8b). At low pressures (e.g., $P < 100$ MPa), the Kratky plot behaves similar to the case of PNIPA solutions. On the other hand, it exhibits a clear peak in the Kratky plot for $P \geq 120$ MPa. Hence, we tried to decompose the $I(q)$ of the 690 mM PNIPA gel to the squared-Lorentz and Lorentz components according to the discussion given in the Theoretical section.

Figure 9 shows the results for the cases of $P = 0.1$ and 170 MPa at 20 °C. $I(q)$'s were decomposed to the Lorentz (L) and squared-Lorentz components (SL) with eq 16. The data for 0.1 MPa has only the L component, while those for 170 MPa have both components and are nicely reconstructed as depicted by the solid line.

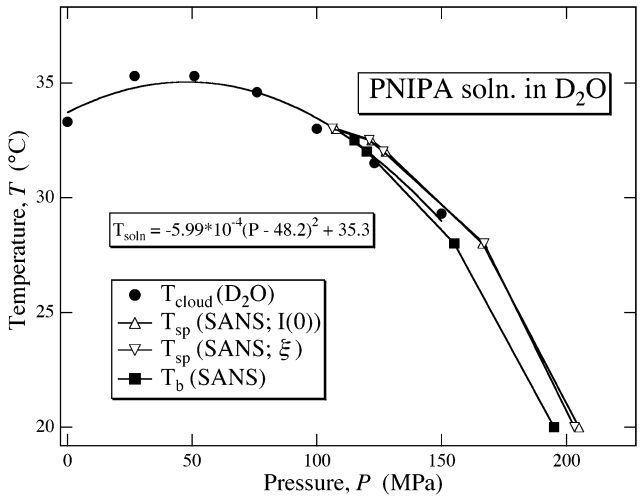

Figure 7. $P-T$ phase diagram of PNIPA solution in D_2O. The binodal, T_b, spinodal, T_{sp}, and cloud point curves, T_{cloud}, are indicated with squares, open (from ξ) and filled triangles (from $I(q = 0)$), and circles, respectively.

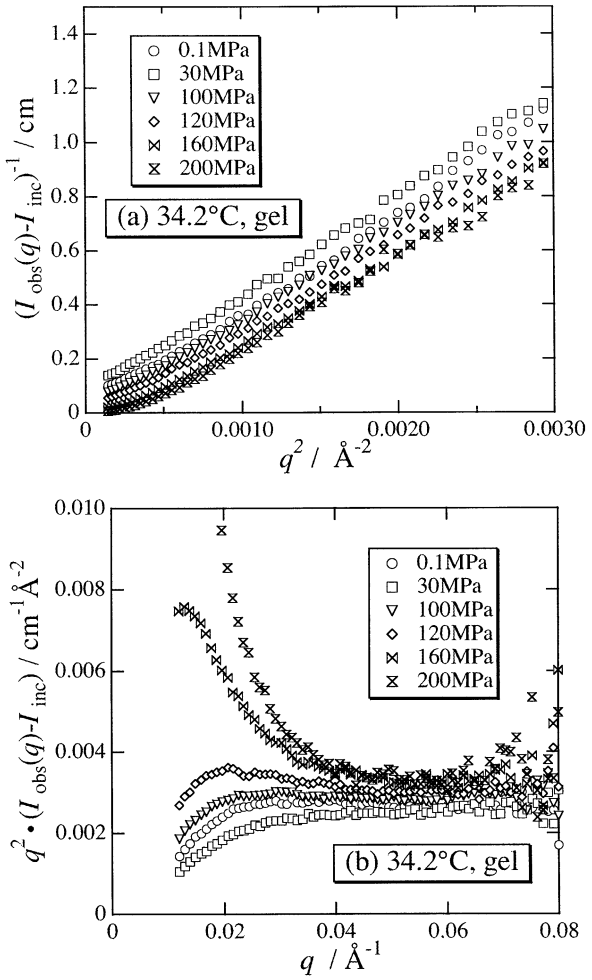

Figure 8. (a) $1/[I(q) - I_{inc}]$ vs q^2 and (b) $q^2[I(q) - I_{inc}]$ plots for PNIPA gels at various pressures. The temperature of observation was 34.2 °C. Note that the Kratky plots have peaks, indicating the presence of a non-Lorentzian component.

Figure 10 shows $I(q)$'s for PNIPA gels at (a) 20, (b) 30, and (c) 34.2 °C at various pressures. Please note that the values of $I(q)_{obs}$'s are much larger than those for PNIPA solutions (Figure 2) and increase with increasing pressure and temperature. After introduction of a SL component, the curve fitting was quite successful, and

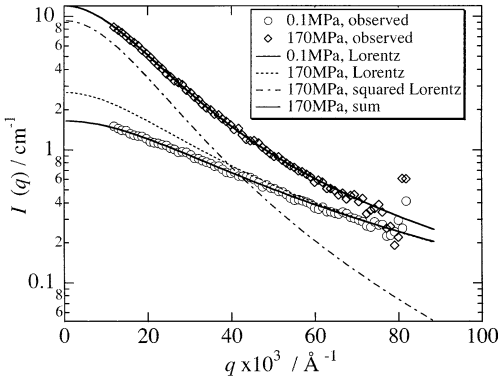

Figure 9. Decomposition plot of $I(q)$ for PNIPA gels in D_2O at 0.1 and 170 MPa. In the case of 0.1 MPa, $I(q)$ is well fitted with a Lorentz function only, while that of 170 MPa needs both components as shown by the dash−dot line (SL) and dashed line (L).

the results are indicated via solid lines, which closely reproduce the observed $I(q)$'s.

Figure 11a shows the variation of $I(0)$ for the gel observed at 20, 30, and 34.2 °C. The scattering intensity increases with increasing pressure. Particularly, $I(0)$ at 34.2 °C seems to diverge. The inset shows the log−log plot of $I(0)$ vs $(P_{sp} - P)/P_{sp}$. Interestingly, although the plot obeys eq 20, the exponent $\gamma_P \geq 7.5$ is significantly large. This indicates that $I(0)$ does not behave as observed in conventional critical phenomena. This is probably due to the static inhomogeneities which diverge with a different fashion. Figure 11b shows the intensity behavior of the dynamic component (i.e., the L component $I_L(0)$). Similarly to $I(0)$, $I_L(0)$ increases with increasing pressure and temperature. This plot is scientifically of significance since we succeeded in decomposing the scattering intensity to the dynamic and static parts. The exponent is $\gamma_P \geq 1.24$. This indicates the L component holds the properties of a polymer solution and behaves similarly as a polymer solution. M_{os} is obtained and plotted as shown in the figure. These values are on the same order as those for the polymer solutions.

Figure 12 shows the fraction of the SL component, X_{SL}, as a function of pressure. In the case of 20 °C, the SANS function is described by only L component up to $P \leq 110$ MPa, and the SL component appears and dominates for $P \geq 110$ MPa. When the temperature was increased to 30 °C, on the other hand, the SL component appears even at atmospheric pressure ($X_{SL} \geq 0.35$) and increases with increasing P. At 34.2 °C, the major component is the static inhomogeneity, i.e., the $I_{SL}(0)$ term. Note that the variation of X_{SL} at 34.2 °C well represents the concave behavior of the $P-T$ phase diagram (bimodal curve) in Figure 1. That is, X_{SL} decreases and then increases with increasing P. The SANS function is dominantly represented by the SL component. This may indicate that the system is in a two-phase region and highly inhomogeneous. Note that $I(0)$ at 20 °C and at 0.1 MPa does not contain the SL term. In general, inhomogeneities, described by a non-Lorentzian behavior, appear by introducing cross-links. However, such inhomogeneities do not appear in as-prepared gels observed at the same condition.[33] Hence, this is a typical example for gels that do not explicitly show inhomogeneities.

Figure 13 shows the critical exponent plots, i.e., ξ vs $(P_{sp} - P)/P_{sp}$, in double logarithmic scale. The critical

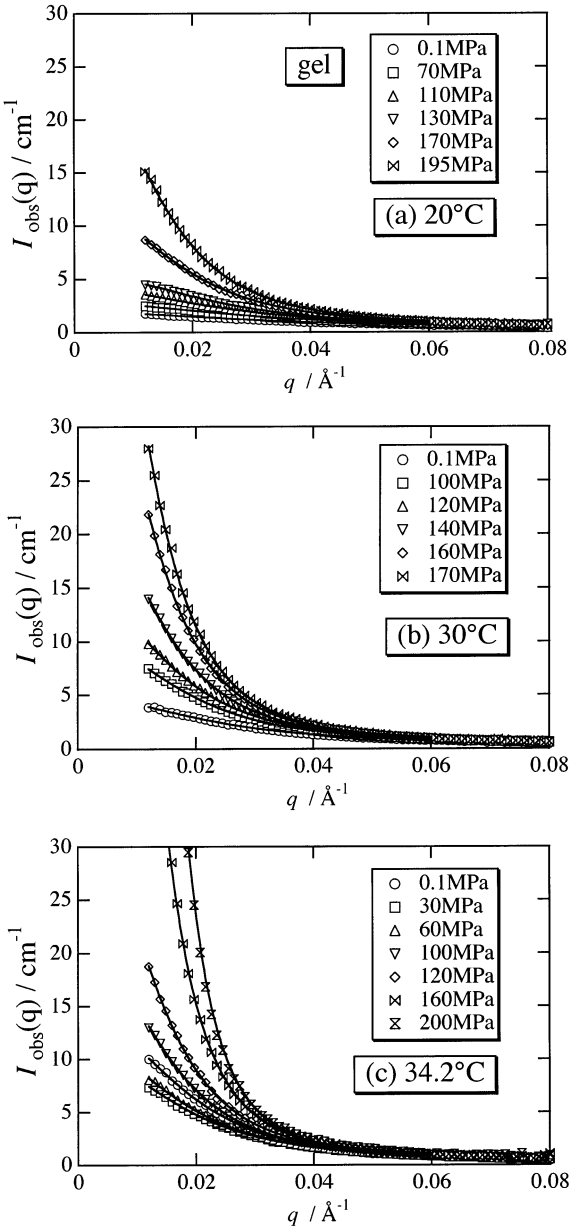

Figure 10. $I(q)$'s for PNIPA gels in D_2O obtained at various pressures obtained at (a) 20, (b) 30, and (c) 34.2 °C. The solid lines are fits with a sum of Lorentz function and squared-Lorentz functions (eq 16 in the text).

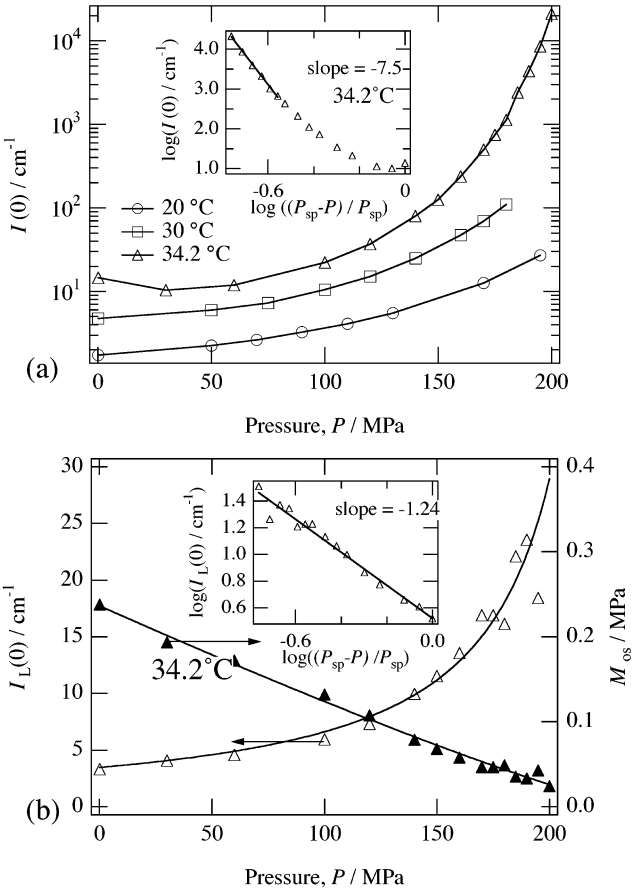

Figure 11. (a) Variation of $I(0)$ with pressure at 20, 30, and 34.2 °C. The inset shows a log−log plot of $I(0)$ vs $(P_{sp} - P)/P_{sp}$. (b) Variation of the dynamic component of scattering intensity, $I_L(0)$, with pressure at 20, 30, and 34.2 °C. The inset shows a log−log plot of $I_L(0)$ vs $(P_{sp} - P)/P_{sp}$. The longitudinal osmotic modulus, M_{os}, evaluated with eq 1 is also plotted with the right axis.

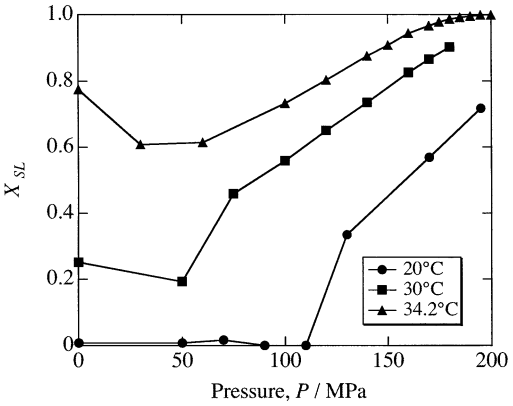

Figure 12. Pressure dependence of the fraction of SL component variation, X_{SL}, for PNIPA gels in D_2O observed at various temperatures.

exponents are thus evaluated to be $\nu_P \geq 0.80$. This value is slightly larger than that expected for an Ising fluid. This may be due to presence of the squared-Lorentz component in the definition of the correlation length in eq 16, which affects its evaluation. In the context of the Rabin−Panyukov theory, one expects that the SL component starts to diverge much earlier than the L component,[34] resulting in smaller critical exponents. However, the results obtained in this work are opposite. This is the first observation of such exponents.

Effects of Cross-Links on Phase Diagram. In this section, we discuss the reentrant phase diagram observed in PNIPA−aqueous systems on the basis of the Hawley theory for the elliptical phase diagram for protein denaturation.[35] This theory is extensively discussed in the recent review by Smeller.[36] As described in Appendix B, the phase boundary is given as an equation for an ellipse

$$\frac{V_0\Delta\beta}{2\Delta G_0}(P - P_0)^2 + \frac{V_0\Delta C_p}{2T_0\Delta G_0}(T - T_0)^2 = 1 \qquad (21)$$

where (P_0, T_0), $\Delta\beta$, and ΔC_p are a reference state, the differences in the isothermal compressibility, and the heat capacity between the one and two phases, respectively. Figure 14 shows the fits of the cloud point curves for PNIPA solutions and gels in H_2O by elliptic functions, and the fitted parameters are given in Table 1. As shown in the figure, the phase diagram can be

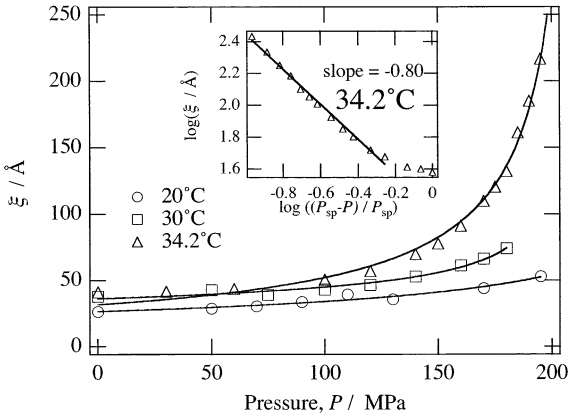

Figure 13. Pressure dependence of ξ at 20, 30, and 34.2 °C. The inset shows a log−log plot of ξ vs $(P_{sp} - P)/P_{sp}$.

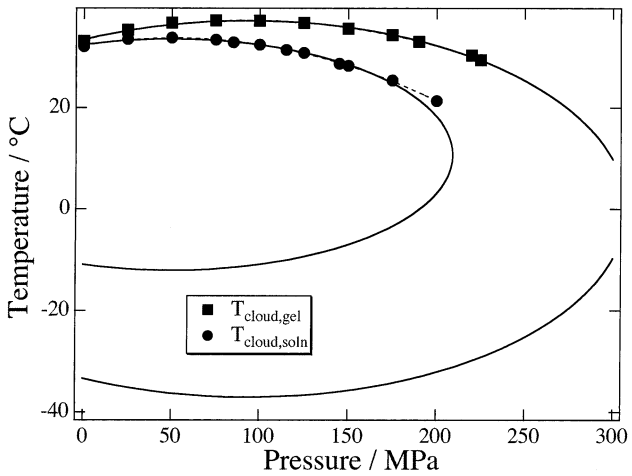

Figure 14. Elliptic phase diagrams for PNIPA solutions and gels.

Table 1. Thermodynamic Parameters Determined for PNIPA Solutions and Gels with Hawley Theory for the Elliptical Phase Diagram

	P_0 (MPa)	T_0 (K)	$V_0\Delta\beta/\Delta G_0$ (MPa^{-2})	$V_0\Delta C_p/\Delta G_0$ (K^{-1})
NIPA soln (H_2O)	49.8	283.8	7.88×10^{-5}	1.092
NIPA gel (H_2O)	93.7	273.2	4.37×10^{-5}	0.398

represented by an ellipse. The centers of ellipses for PNIPA solutions and gels are $(P_0, T_0) = (49.8$ MPa, 284 K) and (93.7 MPa, 273 K) respectively for the solution and gel. ΔG_0 is the free energy at (P_0, T_0). It is rather difficult to discuss the difference in ΔC_p and in $\Delta\beta$ between the PNIPA gels and solution since the reference value of ΔG_0 of the PNIPA solution is different from that of the gel. However, knowing that the enthalpy changes from one- to two-phase for the solution, ΔH_{soln}, and gel, ΔH_{gel}, are significantly different, i.e., $\Delta H_{soln} = 4.8-6.1$ kJ/(mol of NIPA)[37] and $\Delta H_{gel} = 3.95$ kJ/(mol of NIPA),[38] it is expected that $\Delta C_{p,gel}$ is significantly smaller than $\Delta C_{p,soln}$. This speculation is supported by the evaluated values of $\Delta C_p/\Delta G_0$ in Table 1. Similarly, the magnitude of $\Delta\beta/\Delta G_0$ for the gel is smaller than that for the solution, indicating $|\Delta\beta_{gel}| < |\Delta\beta_{soln}|$. This may indicate that gels are less compressible than the corresponding polymer solutions. These results as well as the phase diagram shown in Figure 1 indicate that the one-phase region becomes larger by cross-linking the polymer chains. Hence, cross-links as well as deuterium substitution play a role to stabilize the "native" state. If the larger $I(q)$'s in the gel near the spinodal are ascribed to thermal concentration fluctuations, $|\Delta\beta_{gel}|$ is expected to be larger than $|\Delta\beta_{soln}|$. This is not the case observed experimentally. Hence, the frozen concentration fluctuations, i.e., cross-linking inhomogeneities, are the reason for the larger scattering intensities of the gel than those of the polymer solution, and the intensity component originated from cross-linking inhomogeneities is well represented by a squared-Lorentz function.

Conclusion

The microstructure of poly(*N*-isopropylacrylamide) (PNIPA) D_2O solutions and gels have been investigated by SANS as a function of hydrostatic pressure and temperature. The PNIPA solutions in H_2O have a convex-upward phase diagram in the temperature−pressure ($P-T$) plane, having a maximum at (51.7 MPa, 33.6 °C; H_2O). The SANS intensity function, $I(q)$, was well represented by a Lorentz function, and critical phenomena were observed with increasing P. The critical exponents for ξ and $I(0)$ were obtained to be $\nu_P \geq 0.6$ and $\gamma_P \geq 1.2$, respectively.

Comparing with the PNIPA solutions, the pressure and temperature dependence of the microstructure of PNIPA gels are of interest. (1) The $P-T$ phase diagram shifts upward by introducing cross-links, i.e., in the case of PNIPA gels, which has a maximum at (93.2 MPa, 37.1 °C; H_2O). (2) $I(q)$'s contain a non-Lorentzian component if the environment is changed from its preparation condition. The non-Lorentzian component becomes important with increasing T and/or P. The non-Lorentzian component can be well described by a SL function with the same correlation length as that of the L component as is predicted by the theories of Onuki and of Panyukov−Rabin. (3) The critical exponents could not be evaluated for the total intensity, $I(0)$, but for the Lorentz component, $I_L(0)$, and were $\nu_P \geq 0.80$ and $\gamma_P \geq 1.24$, which more or less recover the exponents for the PNIPA solutions. (4) The $P-T$ phase diagrams were also represented by ellipses. The ellipse of the gel was larger than that of the solution, indicating the "native state", i.e., the one-phase region, of gels is larger than that of polymer solutions. All of these experimental findings are explained by the emergence of frozen inhomogeneities and increase of thermal stability via introduction of permanent cross-linking.

Acknowledgment. This work is partially supported by the Ministry of Education, Science, Sports and Culture, Japan (Grant-in-Aid and 14350493, 14045216 to M.S.). The authors express their thanks to Yitzhak Rabin, Bar-Ilan University, Israel, for valuable discussion and comments. The SANS experiment was performed with the approval of the Institute for Solid State Physics, The University of Tokyo (Proposal No. 03-3503), at Japan Atomic Energy Research Institute, Tokai, Japan. This work is also supported by Core Research for Evolutional Science and Technology (CREST), Japan Science and Technology Agency, Japan.

Appendix A

The correlator of thermal fluctuations is given by

$$G_{\mathbf{q}} = \frac{1}{g_{\mathbf{q}}^{-1} + w} \tag{A1}$$

On the other hand, the static correlator can be written as

$$C_{\mathbf{q}} = \left(\frac{1}{g_{\mathbf{q}}^{-1} + w}\right)^2 \frac{\nu_{\mathbf{q}}}{g_{\mathbf{q}}^{2}} \tag{A2}$$

Now let us write

$$g_{\mathbf{q}} = g_{\mathbf{q}1} + g_{\mathbf{q}2} \tag{A3}$$

where

$$g_{\mathbf{q}1} = \frac{1}{\frac{Q^2}{2} + \frac{1}{4Q^2} + 1}, \quad g_{\mathbf{q}2} = \frac{2}{(1+Q^2)^2\left(\frac{\phi_0}{\phi}\right)^{2/3}} \tag{A4}$$

Let us consider the different limits

$$g_{\mathbf{q}1} \rightarrow \begin{cases} 2/Q^2 & Q \gg 1 \\ 4Q^2 & Q \ll 1 \end{cases} \tag{A5a}$$

and

$$g_{\mathbf{q}2} \rightarrow \begin{cases} 2(\phi/\phi_0)^{2/3}/Q^4 & Q \gg 1 \\ 2(\phi/\phi_0)^{2/3} & Q \ll 1 \end{cases} \tag{A5b}$$

Therefore

$$g_{\mathbf{q}}^{-1} \rightarrow \begin{cases} g_{\mathbf{q}1}^{-1} = Q^2/2 & Q \gg 1 \\ g_{\mathbf{q}2}^{-1} = \frac{1}{2}(\phi_0/\phi)^{2/3} & Q \ll 1 \end{cases} \tag{A6}$$

and therefore a uniform approximation for $g_{\mathbf{q}}$ would be

$$g_{\mathbf{q}} \cong \frac{2}{(\phi_0/\phi_0)^{2/3} + Q^2} \tag{A7}$$

Note that $G_{\mathbf{q}}$ becomes a Lorentzian:

$$G_{\mathbf{q}} \cong \frac{2}{(\phi_0/\phi)^{2/3} + Q^2 + 2w} = \frac{S_{\mathrm{L}}(0)}{1 + \xi^2 q^2} \tag{A8}$$

where

$$\xi = \frac{a N_{\mathrm{X}}^{1/2}}{\sqrt{12\left[w + \frac{1}{2}\left(\frac{\phi_0}{\phi}\right)^{2/3}\right]}} \tag{A9}$$

Now let us examine the small and large Q limits of $\nu_{\mathbf{q}}/g_{\mathbf{q}}^2$. We write

$$\frac{\nu_{\mathbf{q}}}{g_{\mathbf{q}}^{2}} \cong \frac{\phi N_{\mathrm{X}}\left\{6 + \frac{9}{w_0 - 1 + (1/2)(\phi_0/\phi)^{2/3}Q^2}\right\}}{(1+Q^2)^2\left\{\frac{2}{(\phi_0/\phi)^{2/3} + Q^2}\right\}^2} \tag{A10}$$

$$\frac{\nu_{\mathbf{q}}}{g_{\mathbf{q}}^{2}} \rightarrow \begin{cases} \frac{3}{2}\phi N_{\mathrm{X}} & Q \gg 1 \\ \frac{3}{2}\phi N_{\mathrm{X}}\left(\frac{\phi_0}{\phi}\right)^{4/3}\left\{1 + \frac{3}{2(w_0 - 1)}\right\} & Q \ll 1 \end{cases} \tag{A11}$$

In the case of as-prepared sample ($\phi = \phi_0$) away from the cross-link saturation threshold ($w_0 \gg 1$), the function tends to be the same value ($3\phi N_{\mathrm{X}}/2$) in both limits. Therefore, the structure factor is given by a sum of Lorentzian and squared Lorentzian, i.e.

$$S_{\mathbf{q}} \cong \frac{S_{\mathrm{L}}(0)}{1 + \xi^2 q^2} + \frac{S_{\mathrm{SL}}(0)}{(1 + \xi^2 q^2)^2} \tag{A12}$$

Appendix B

The free energy difference of PNIPA solutions and gels between one and two phases, ΔG, is given by

$$\Delta G = G_{\text{two phases}} - G_{\text{one phase}} \tag{B1}$$

The one- and two-phases correspond to the native and denatured states, respectively. Since the free energy is a function of pressure as well as temperature, let us expand the free energy difference in a power series as follows

$$\Delta G = \frac{1}{2}\left(\frac{\partial^2 \Delta G}{\partial P^2}\right)_0 (P - P_0)^2 + \left(\frac{\partial^2 \Delta G}{\partial P\, \partial T}\right)_0 (P - P_0) \times (T - T_0) + \frac{1}{2}\left(\frac{\partial^2 \Delta G}{\partial T^2}\right)_0 (T - T_0)^2 + \left(\frac{\partial \Delta G}{\partial P}\right)_0 (P - P_0) + \left(\frac{\partial \Delta G}{\partial T}\right)_0 (T - T_0) + \Delta G_0 \tag{B2}$$

where (P_0, T_0) is a reference state. Since the first and second derivatives of ΔG are related to the thermodynamic quantities, i.e.

$$\left(\frac{\partial G}{\partial P}\right)_T = V, \quad \left(\frac{\partial G}{\partial T}\right)_P = -S \tag{B3}$$

$$\alpha = \frac{1}{V}\left(\frac{\partial V}{\partial T}\right)_P = -\frac{1}{V}\left(\frac{\partial S}{\partial P}\right)_T, \quad \beta = -\frac{1}{V}\left(\frac{\partial V}{\partial P}\right)_T, \quad C_p = \frac{T}{V}\left(\frac{\partial S}{\partial T}\right)_P \tag{B4}$$

where S is the entropy, V is the volume, α is the thermal expansion coefficient, β is the isothermal compressibility, and C_p is the heat capacity per unit volume.

$$\Delta G = -\frac{V_0 \Delta\beta}{2}(P - P_0)^2 + V_0 \Delta\alpha (P - P_0)(T - T_0) - \frac{V_0 \Delta C_p}{2T_0}(T - T_0)^2 + \Delta V_0 (P - P_0) - \Delta S_0 (T - T_0) + \Delta G_0 \tag{B5}$$

This equation indicates that the phase boundary has the form of an ellipse. By choosing the reference point to be the center of ellipse, one gets

$$\Delta G = -\frac{V_0 \Delta\beta}{2}(P - P_0)^2 - \frac{V_0 \Delta C_p}{2T_0}(T - T_0)^2 + \Delta G_0 \tag{B6}$$

Hence

$$\frac{V_0 \Delta\beta}{2\Delta G_0}(P - P_0)^2 + \frac{V_0 \Delta C_p}{2T_0 \Delta G_0}(T - T_0)^2 = 1 \tag{B7}$$

References and Notes

(1) Tanaka, T. *Sci. Am.* **1981**, *244*, 110.
(2) Shibayama, M.; Tanaka, T. *Adv. Polym. Sci.* **1993**, *109*, 1.
(3) Hirokawa, Y.; Tanaka, T. *J. Chem. Phys.* **1984**, *81*, 6379.
(4) Tanaka, T.; Fillmore, D. J.; Sun, S. T.; Nishio, I.; Swislow, G.; Shah, A. *Phys. Rev. Lett.* **1980**, *45*, 1636.
(5) Tanaka, T. *Polymer* **1979**, *20*, 1404.
(6) Tanaka, T. *Phys. Rev. Lett.* **1978**, *40*, 820.
(7) Kato, E.; Kitada, T. *J. Phys. Soc. Jpn.* **1994**, *63*, 2831.

(8) Kato, E. *J. Chem. Phys.* **1997**, *106*, 3792.
(9) Nakamoto, C.; Kitada, T.; Kato, E. *Polym. Gels Networks* **1996**, *4*, 17.
(10) Tanford, C. *Physical Chemistry of Macromolecules*; Wiley: New York, 1961.
(11) Otake, K.; Karaki, R.; Ebina, T.; Yokoyama, C.; Takahashi, S. *Macromolecules* **1993**, *26*, 2194.
(12) Kato, E.; Kitada, T.; Nakamoto, C. *Macromolecules* **1993**, *26*, 1758.
(13) Rebelo, L. P. N.; Visak, Z. P.; de Sousa, H. C.; Szydlowski, J.; Gomes de Azevedo, R.; Ramos, A. M.; Najdanovic-Visak, V.; Nunes da Ponte, M.; Klein, J. *Macromolecules* **2002**, *35*, 1887.
(14) Kunugi, S.; Takano, K.; Tanaka, N. *Macromolecules* **1997**, *30*, 4499−4501.
(15) Kunugi, S.; Tanaka, N. *Biochim. Biophys. Acta* **2002**, *1595*, 329.
(16) Shibayama, M. *Macromol. Chem. Phys.* **1998**, *199*, 1.
(17) Panyukov, S.; Rabin, Y. *Phys. Rep.* **1996**, *269*, 1.
(18) de Gennes, P. G. *J. Phys., Lett.* **1979**, *40*, L69.
(19) Onuki, A. *J. Phys. II* **1992**, *2*, 45.
(20) Onuki, A. *Phase Transition Dynamics*; Cambridge University Press: Cambridge, 2002.
(21) Geissler, E.; Horkay, F.; Hecht, A. M.; Rochas, C.; Lindner, P.; Bourgaux, C.; Couarraze, G. *Polymer* **1997**, *38*, 15.
(22) Stanley, H. E. *Introduction to Phase Transition and Critical Phenomena*; Oxford University Press: New York, 1971.
(23) Li, Y.; Tanaka, T. *J. Chem. Phys.* **1989**, *90*, 5161.
(24) Shibayama, M.; Tanaka, T.; Han, C. C. *J. Chem. Phys.* **1992**, *97*, 6829.
(25) Ito, Y.; Imai, M.; Takahashi, S. *Physica B* **1995**, *213&214*, 889.
(26) Nagao, M.; Okabe, S.; Karino, T.; Shibayama, M. Manuscript in preparation.
(27) Matsumoto, M.; Murakoshi, K.; Wada, Y.; Yanagida, S. *Chem. Lett.* **2000**, 938.
(28) Schwahn, D.; Takeno, H.; Willner, L.; Hasegawa, H.; Jinnai, H.; Hashimoto, T.; Imai, M. *Phys. Rev. Lett.* **1994**, *73*, 3427.
(29) Kato, E. *J. Appl. Polym. Sci.*, submitted for publication.
(30) Shirota, H.; Kuwabara, N.; Ohkawa, K.; Horie, K. *J. Phys. Chem. B* **1999**, *103*, 10400.
(31) Bates, F. S.; Wignall, G. D.; Koehler, W. C. *Phys. Rev. Lett.* **1985**, *55*, 2425.
(32) Buckingham, A. D.; Hentschel, H. G. E. *J. Polym. Sci., Polym. Phys. Ed.* **1980**, *18*, 853.
(33) Baumgartner, A., Picot, C. E., Eds. *Molecular Basis of Polymer Networks*; Springer: Berlin, 1989; Vol. 42.
(34) Shibayama, M.; Kawakubo, K.; Norisuye, T. *Macromolecules* **1998**, *31*, 1608.
(35) Hawley, S. A. *Biochemistry* **1971**, *10*, 2436.
(36) Smeller, L. *Biochim. Biophys. Acta* **2002**, *1595*, 11.
(37) Otake, K.; Inomata, H.; Konno, M.; Saito, S. *Macromolecules* **1990**, *23*, 283.
(38) Shibayama, M.; Mizutani, S.; Nomura, S. *Macromolecules* **1996**, *29*, 2019.

MA0359685